to the presence or absence of *MYCN* amplification. Figure 3a shows that the 5-year survival rates of patients with GGSs ($n=18$), GGWs ($n=33$) and GGPs ($n=25$) tumors were 89, 85 and 53%, respectively, whereas those of patients with GGSa ($n=5$), GGWa ($n=3$) and GGPa ($n=28$) tumors involving *MYCN* amplification were 0, 33 and 34%, respectively (Figure 3b). We then further examined the survival curves of patients with *MYCN*-nonamplified tumors in young (<1-year-old) and old (≥1-year-old) patients. Figure 3c shows the 5-year survival rates of 88, 86 and 67% in GGWs ($n=24$), GGSs ($n=7$) and GGPs ($n=3$) tumors, respectively, among young patients, whereas they were 76, 91 and 51% in GGWs ($n=9$), GGSs ($n=11$) and GGPs ($n=22$) tumors, respectively, among old patients (Figure 3d). The former pattern was similar to that in MS-detected tumors, which had high percentages of GGW tumors, whereas the latter contained high incidences of GGP tumors.

Table 1 Five-year overall survival rates of the patients with each genomic subgroup of sporadic neuroblastomas

	N	*5-Year OS (%)*
GGS		
GGSa	5	0
GGSs	18	89
GGP		
GGP1a	22	44
GGP1s	2	0
GGP2a	4	0
GGP2s	5	40
GGP3a	1	0
GGP3s	15	59
GGP4a	1	0
GGP4s	3	67
GGW		
GGW1a	0	—
GGW1s	0	—
GGW2a	0	—
GGW2s	1	100
GGW3a	0	—
GGW3s	3	100
GGW4a	1	0
GGW4s	23	87
GGW5a	2	50
GGW5s	6	67

Abbreviations: GGP, partial chromosomal gains/losses genomic group; GGS, silent genomic group; GGW, whole gains and/or losses genomic group; OS, overall survival rate.

Segregation of the prognosis of sporadic neuroblastomas with a single copy of MYCN by genomic and molecular signatures

Recently, we have generated a clinically useful cDNA microarray carrying 200 genes that predicts the prognosis of neuroblastomas with an accuracy rate of 89% (Ohira *et al.*, 2005). The univariate analysis of 112 sporadic neuroblastomas showed that both genomic signatures (GGP vs GGW + GGS, $P=0.003$) and molecular signatures (posterior value<0.5 vs ≥0.5, $P<0.001$) were highly significant prognostic indicators, like other variables including age ($P=0.006$), stage ($P<0.001$), tumor origin ($P=0.001$), *TrkA* expression ($P=0.004$), Shimada classification ($P<0.001$) and *MYCN* amplification ($P<0.001$; Table 2). In addition, genomic signature was a prognostic factor independent from molecular signature, age and tumor origin, although it showed no prognostic significance when stage, Shimada classification, or *MYCN* amplification was controlled (Table 2). Even in sporadic neuroblastomas with a single copy of *MYCN*, the highest significance according to the univariate analysis was given to molecular signature ($P=0.002$), followed by tumor origin ($P=0.006$) and genomic signature ($P=0.010$; Table 2). The multivariate analysis also showed that genomic signature was a prognostic indicator independent from molecular signature or tumor origin (Table 2). As shown in Figure 4, our in-house expression microarrays segregated the survival curves of patients with sporadic tumors lacking *MYCN* amplification (GGSs + GGPs + GGWs) into the favorable (94%, $n=17$) and unfavorable (42%, $n=13$) prognosis groups ($P=0.001$).

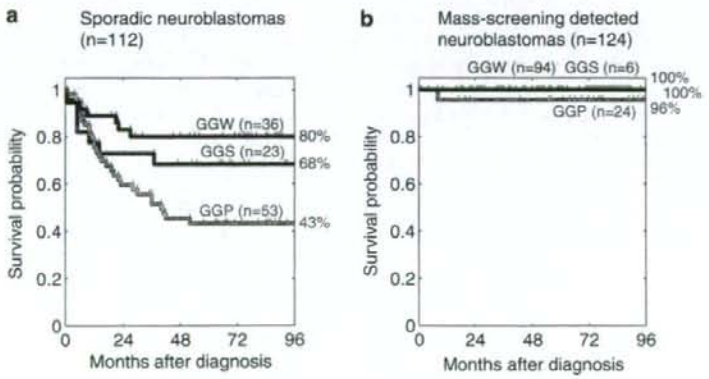

Figure 2 Kaplan–Meier survival curves in three genomic groups (GGS, GGP and GGW) based on array-CGH. (**a**) Sporadic neuroblastomas: GGS vs GGP: $P=0.109$, GGS vs GGW: $P=0.320$ and GGP vs GGW: $P=0.002$. (**b**) Mass screening-detected neuroblastomas: GGS vs GGP: $P=1.000$, GGS vs GGW: $P=1.000$ and GGP vs GGW: $P=1.000$.

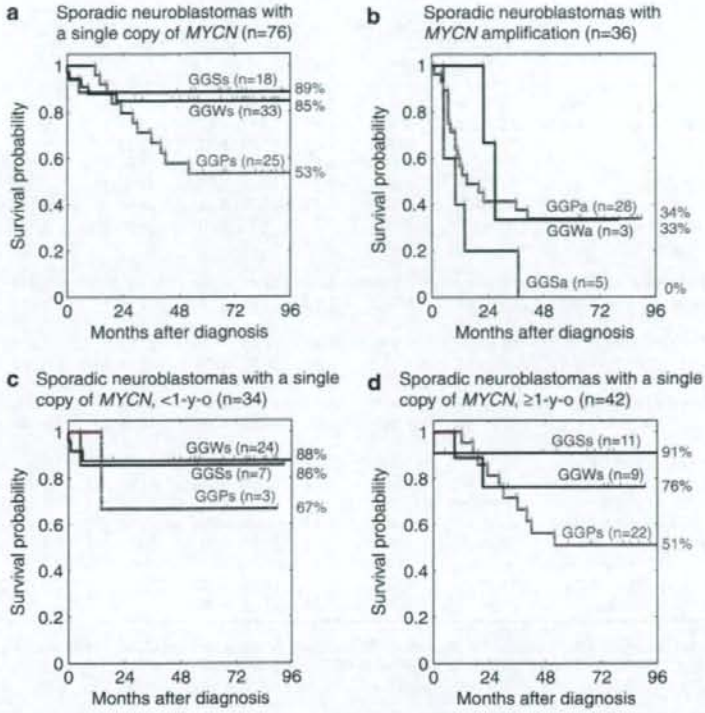

Figure 3 Kaplan–Meier survival curves in three genomic groups (GGS, GGP and GGW) of sporadic neuroblastomas based on array-CGH. (**a**) Sporadic neuroblastomas with a single copy of *MYCN* GGS vs GGP: $P=0.035$, GGS vs GGW: $P=0.736$ and GGP vs GGW: $P=0.033$. (**b**) Sporadic neuroblastomas with *MYCN* amplification GGS vs GGP: $P=0.104$, GGS vs GGW: $P=0.156$ and GGP vs GGW: $P=0.642$. (**c**) Sporadic neuroblastomas with a single copy of *MYCN* in patients under 1 year of age GGS vs GGP: $P=1.000$, GGS vs GGW: $P=0.919$ and GGP vs GGW: $P=0.412$. (**d**) Sporadic neuroblastomas with a single copy of *MYCN* in patients over 1 year of age. GGS vs GGP: $P=0.063$, GGS vs GGW: $P=0.478$ and GGP vs GGW: $P=0.481$.

Discussion

The present array-CGH analysis revealed the whole feature of the genomic abnormality patterns of sporadic and MS-detected neuroblastomas. The patterns of genomic aberrations in MS-detected neuroblastomas are similar to those in sporadic tumors, suggesting that they are genetically genuine neuroblastomas which are similar to sporadic tumors found in patients under 1 year of age. Indeed, both of them have a high tendency to regress spontaneously. The exceptions we found are that the incidence of GGPs tumors is relatively higher in MS-detected tumors than in sporadic tumors found among young patients and that their clinical outcome is very good.

BAC array-based aCGH analyses have defined several minimal critical regions of gains and losses in 1p, 2p and 11q. These included minimal losses in 10 Mb regions of 1p36.3 (1pter to RP11-199O1, *D1S244*) and 11q23 (from RP11-42L18 to RP11-45N4). The 2 Mb region in 1p36.2–36.3 detected by a BAC clone RP11-219F4 (*D1S507*) exhibited highest deletion frequency of 32%. By combining the expression data obtained by the in-house microarrays harboring approximately 5340 genes derived from primary neuroblastomas, several candidate genes including *CHD5* at 1p36 (Bagchi *et al.*, 2007) as well as *Survivin* at 17q25 (Islam *et al.*, 2000) were identified as lowly and highly expressed genes in neuroblastomas with advanced stages, respectively (manuscript in preparation). The amplicon surrounding the *MYCN* locus was ranged from 2.4 Mb proximal (*G14110*) to 5 Mb distal (*D2S387*) of *MYCN* itself and gains were further extended to wider range, from 2pter to 2p11.

To date, the presence of the GGS subgroup with very silent aberrations of the tumor genome has never been verified definitely. The distribution of GGS tumors is very unique; namely, they are present in both MS detected and sporadic tumors removed from the patients under 1 year of age. They are also found in tumors obtained from the patients over 1 year of age, and some of them possess *MYCN* amplification. Furthermore, GGS tumors mostly show diploid karyotype. These facts suggest that GGSs tumors might represent neuroblastoma at an early stage of carcinogenesis with early oncogenic hit(s), which later develop to GGP or

Table 2 Univariate and multivariate analyses of genomic and molecular signature as well as other prognostic factors in sporadic neuroblastomas

	Sporadic NBLs (all cases)				*Sporadic NBLs (MYCN, single copy)*			
	N	P	*HR*	*CI*	N	P	*HR*	*CI*
Genomic signature (GGP vs GGW+GGS)	53 vs 59	0.003	2.59	(1.36, 4.90)	25 vs 51	0.010	3.41	(1.32, 8.82)
Molecular signature (posterior <0.5 vs $\geqslant 0.5$)	22 vs 18	<0.001	11.15	(2.52, 49.35)	13 vs 17	0.002	14.05	(1.72, 114.89)
Age ($\geqslant$1-year old vs $<$1-year old)	74 vs 38	0.006	2.67	(1.24, 5.77)	42 vs 34	0.070	2.47	(0.88, 6.96)
Stage (3, 4 vs 1, 2, 4 s)	73 vs 38	<0.001	4.92	(1.93, 12.54)	38 vs 37	0.038	2.80	(1.00, 7.88)
Origin (adrenal vs nonadrenal)	72 vs 40	0.001	3.22	(1.43, 7.25)	41 vs 35	0.006	4.59	(1.33, 15.85)
TRKA expression (low vs high)	52 vs 36	0.004	3.37	(1.36, 8.34)	24 vs 36	0.766	1.21	(0.34, 4.31)
Shimada (unfavorable vs favorable)	39 vs 37	<0.001	4.54	(1.71, 12.07)	14 vs 36	0.668	1.37	(0.33, 5.75)
MYCN (amplification vs single copy)	36 vs 75	<0.001	3.98	(2.16, 7.35)	—	—	—	—
Genomic signature (GGP vs GGW+GGS)	15 vs 25	0.045	2.89	(1.01, 8.30)	8 vs 22	0.031	5.46	(1.09, 27.40)
Molecular signature (posterior <0.5 vs $\geqslant 0.5$)	22 vs 18	0.002	7.52	(1.69, 33.38)	13 vs 17	0.034	7.41	(0.90, 60.87)
Genomic signature (GGP vs GGW+GGS)	53 vs 59	0.048	1.99	(1.05, 3.78)	25 vs 51	0.055	2.85	(1.10, 7.36)
Age ($\geqslant$1-year old vs $<$1-year old)	74 vs 38	0.132	1.88	(0.87, 4.06)	42 vs 34	0.549	1.44	(0.51, 4.05)
Genomic signature (GGP vs GGW+GGS)	53 vs 58	0.416	1.34	(0.71, 2.54)	25 vs 50	0.098	2.61	(1.01, 6.76)
Stage (3, 4 vs 1, 2, 4 s)	73 vs 38	0.005	4.06	(1.60, 10.34)	38 vs 37	0.496	1.56	(0.56, 4.40)
Genomic signature (GGP vs GGW+GGS)	53 vs 59	0.012	2.23	(1.18, 4.23)	25 vs 51	0.015	3.19	(1.23, 8.26)
Origin (adrenal vs non-adrenal)	72 vs 40	0.006	2.78	(1.24, 6.26)	41 vs 35	0.008	4.30	(1.24, 14.88)
Genomic signature (GGP vs GGW+GGS)	41 vs 47	0.079	2.17	(0.96, 4.95)	18 vs 42	0.050	3.75	(1.06, 13.33)
TRKA expression (low vs high)	52 vs 36	0.078	2.34	(0.95, 5.79)	24 vs 36	0.727	0.79	(0.22, 2.80)
Genomic signature (GGP vs GGW+GGS)	53 vs 58	0.236	1.53	(0.81, 2.90)	—	—	—	—
MYCN (amplification vs single copy)	36 vs 75	<0.001	3.30	(1.79, 6.08)	—	—	—	—

Abbreviations: CI, confidence interval; GGP, partial chromosomal gains/losses genomic group; GGS, silent genomic group; GGW, whole gains and/or losses genomic group; HR, hazard ratio; *N*, sample number; NBLs, neuroblastomas; *P*, *P*-value.

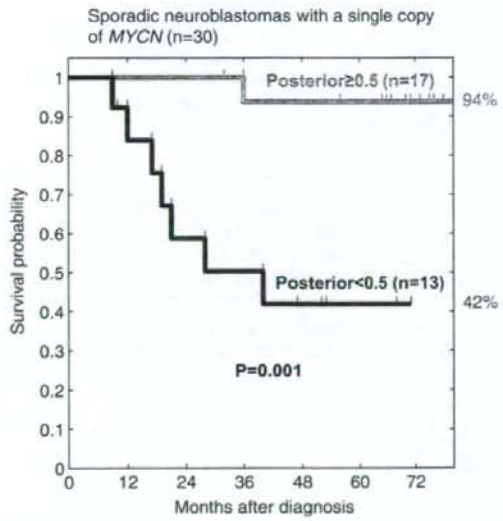

Figure 4 Kaplan–Meier survival curves of sporadic neuroblastomas with a single copy of *MYCN* according to the molecular signature. Gene-expression profiling segregated patients into the favorable (posterior score $\geqslant 0.5$) and unfavorable (posterior score <0.5) prognosis groups ($P=0.001$). The posterior score denotes how likely the patient would show good outcome after 5 years (Ohira *et al*., 2005).

GGW tumors. Since MS did not decrease the incidence of sporadic neuroblastomas (Brodeur *et al*., 2001; Levy, 2005), GGSs tumors in young and old patients might be derived from different progenitor cells. It is interesting that the clinical outcome is very good for patients with *MYCN*-nonamplified GGSs tumors, whereas it is very bad for patients with GGSa tumors possessing *MYCN* amplification, implying again remarkable impact of *MYCN* amplification on the patient's outcome.

The GGP group is characterized by the presence of 17q gain with other chromosomal abnormalities including *MYCN* amplification, 1p loss and 11q loss. Since this group of tumors shows multiple chromosomal aberrations with partial gains and/or losses, unknown causes to induce genomic instability might have triggered genesis of neuroblastoma in progenitor or stem cells of sympathetic cell lineage (Maris and Matthay, 1999; Nakagawara, 2004). The frequently observed GGP tumors are as follows: GGP1a tumors with both 1p loss and *MYCN* amplification and GGP3s tumors with 11q loss but without *MYCN* amplification. The former may belong to a typical *MYCN*-amplified neuroblastoma (White *et al*., 1995) with a 5-year cumulative survival rate of 42% in our series, whereas the latter to the so-called intermediate type tumor (Srivatsan *et al*., 1993; Attiyeh *et al*., 2005) with the rate of 75%. In GGP tumors, it is obvious that *MYCN* amplification has the most powerful impact on the patient prognosis. Interestingly, among the GGPs tumors lacking *MYCN* amplification, 1p loss and 11q loss seem to similarly affect the prognosis. However, GGP2s tumors with both 1p loss and 11q loss show poorer prognosis in an additive manner. The similar additive effect has also been observed in GGP1a (42%

survival) and GGP2a (0% survival) with *MYCN*-amplified tumors. These suggest that 1p loss and 11q loss may independently affect the outcomes of neuroblastoma. Interestingly, one of the main characteristics of the *MYCN*-amplified tumors found in the long-term survivors is a lack of 11q loss (Supplementary Figure S4), corresponding to the observation that the high percentage of 5-year survival rate is shown in the GGP1a group with 1p loss but without 11q loss.

GGW neuroblastoma has a favorable prognosis, as reported (Vandesompele *et al*., 1998). Since the pattern of chromosomal aberrations is represented by whole chromosomal gains and/or losses, mitotic dysfunction during the cell division cycle in progenitor or stem cells might have generated neuroblastoma (Maris and Matthay, 1999; Nakagawara, 2004). Interestingly, 1p loss or 11q loss in a minor population of GGWs tumors (GGW1s and GGW3s) seems not to affect the prognosis.

The presence of different patterns of genomic aberrations like GGS, GGP and GGW may reflect differences in stem or progenitor cells targeted to generate different genetic subsets of neuroblastomas. Although carcinogenic events to cause neuroblastomas may occur sequentially (Tonini, 1993), our serial analyses of six paired primary and recurrent tumors interestingly suggest that the major genetic events, for example, *MYCN* amplification, 1p loss, 11q loss and 17q gain, could occur not always in order during tumor progression (Supplementary Table S3).

Thus, the genomic signatures presented here successfully categorized new prognostic subgroups of neuroblastomas. The rather consistent patterns of genomic abnormalities provide reliable information to understanding of the genetic bases which underlie the clinical phenotypes of neuroblastomas with different survival rates. However, the pattern of genomic abnormalities may often lack biological significance affecting the clinical behavior of individual tumors. The gene-expression profile well reflects the biology of individual tumor. Therefore, establishment of the combined system of both genomic and molecular signatures is ideal for predicting the prognosis of individual patients with neuroblastoma. The present study has clearly shown that genomic and molecular signatures are independent prognostic indicators and suggests that an expression microarray could compensate for the relevant lack when used only genomic signature. In conclusion, combined genomic and molecular signatures may be clinically useful for constituting an ideal system to categorize and even individualize each tumor, which may make tailored medicine of neuroblastoma possible.

Materials and methods

Patients, tissue specimens and DNA/RNA resources

Tumor specimens were collected from 236 patients who had undergone biopsy or surgery at various institutions in Japan (see Supplementary Information). They included 112 sporadic and 124 MS-detected neuroblastoma specimens. All tumors were histopathologically diagnosed as neuroblastoma or ganglioneuroblastoma and were staged according to the International Neuroblastoma Staging System (Brodeur *et al*., 1993). Informed consent was obtained at each institution or hospital. The procedure of this study was approved by the Institutional Review Board of the Chiba Cancer Center (CCC7817). Patients were treated by the standard protocols (Kaneko *et al*., 2002; Iehara *et al*., 2006) in Japan between 1995 and 2003. All MS-detected tumors were diagnosed between 6 and 8 months after birth by measuring urinary catecholamine metabolites in Japan (Sawada *et al*., 1984). Fresh neuroblastoma tissues removed during surgery were stored at −80°C. *MYCN* copy number, *TrkA* mRNA expression and DNA ploidy were measured as reported previously (Islam *et al*., 2000).

Microarray-based comparative genomic hybridization

A chip carrying 2464 BAC clones prepared by ligation-mediated PCR, which covers the whole human genome at roughly 1.2-Mb resolution (Snijders *et al*., 2001; Albertson *et al*., 2003), was used. The 500-ng aliquots of tumors and reference DNAs were labeled by random priming with each Cy3-dCTP and Cy5-dCTP (Amersham Pharmacia, Piscataway, NJ, USA). Hybridization was performed as previously reported (Pinkel *et al*., 1998). UCSF Spot and UCSF Sproc programs to analyse values for spotted clones (Jain *et al*., 2002) were used. All array-CGH data are available at NCBI Gene Expression Omnibus (GEO, http://www.ncbi.nlm.nih.gov/geo/) with accession number GSE 5784.

cDNA microarrays

In-house cDNA microarrays, carrying 5340 cDNAs obtained from the oligo-capping cDNA libraries generated from anonymous neuroblastoma tissues (Ohira *et al*., 2003, 2005), were used. Preparation of RNA, hybridization, reading of spots and statistical analyses were conducted as reported previously (Ohira *et al*., 2005). Gene-expression profile data described in this study is available at NCBI GEO with accession number GSE 5779.

Statistical analysis

The fluorescence ratio for each array CGH spot was normalized and rescaled into estimated copy number aberrations of each clone according to the comb-fit method (Oba *et al*., 2006; see also Supplementary Figure S2a). Chromosomal events were detected by locally smoothing variations in copy number aberrations of clones on a chromosome and by applying threshold rules (see Supplementary Figure S2a and Supplementary Information for more detail). The numbers of whole chromosomal events, Nw and of partial chromosomal events, Np, were counted for $22+2$ chromosomes in every specimen, and the scatter plot in the Nw–Np plane exhibited apparent three clusters: whole differential dominant ($Nw > Np$), partial differential dominant ($Nw < Np$) and silent ($Nw \approx 0$, $Np \approx 0$) (Supplementary Figure S2b). To discriminate whole differential dominant from partial differential dominant, we defined a 'global' feature variable α as computationally evaluated as the ratio between Nw and Np; when α was small (large), the sample was likely to be whole (partial) differential dominant (see Supplementary Information for more detail). A differential analysis of gene expression was made using standard *t*-test with the *q*-value analysis (Storey and Tibshirani, 2003) for incorporating a false discovery rate (to deal with multiple statistical tests). A survival analysis was made based on Kaplan–Meier and log-rank tests. Univariate and multivariate analyses were made according to the Cox hazard models.

Acknowledgements

We thank institutions and hospitals for providing tumor specimens (see Supplementary Information). We also thank Shigeru Sakiyama, Hiroki Nagase, Iwao Nozawa, Tadayuki Koda and technical staff, past and present, at Division of Biochemistry, Chiba Cancer Center Research Institute. We acknowledge Hisamitsu Pharmaceutical Co. Inc., the Ministry of Education, Culture, Sports, Science and Technology of Japan, the Ministry of Health, Labour and Welfare of Japan and the Hamaguchi Foundation for the Advancement of Biochemistry for funding this work.

References

Albertson DG, Collins C, McCormick F, Gray JW. (2003). Chromosome aberrations in solid tumors. *Nat Genet* **34**: 369–376.

Attiyeh EF, London WB, Mosse YP, Wang Q, Winter C, Khazi D *et al.* (2005). Chromosome 1p and 11q deletions and outcome in neuroblastoma. *N Engl J Med* **353**: 2243–2253.

Bagchi A, Papazoglu C, Wu Y, Capurso D, Brodt M, Francis D *et al.* (2007). CHD5 is a tumor suppressor at human 1p36. *Cell* **128**: 459–475.

Beckwith JB, Perrin EV. (1963). *In situ* neuroblastomas: a contribution to the natural history of neural crest tumors. *Am J Pathol* **43**: 1089–1101.

Brodeur GM. (2003). Neuroblastoma: biological insight into a clinical enigma. *Nat Rev Cancer* **3**: 203–216.

Brodeur GM, Look AT, Shimada H, Hamilton VM, Maris JM, Hann HW *et al.* (2001). Biological aspects of neuroblastomas identified by mass screening in Quebec. *Med Pediatr Oncol* **36**: 157–159.

Brodeur GM, Pritchard J, Berthold F, Carlsen NL, Castel V, Castelberry RP *et al.* (1993). Revisions of the international criteria for neuroblastoma diagnosis, staging, and response to treatment. *J Clin Oncol* **11**: 1466–1477.

Iehara T, Hosoi H, Akazawa K, Matsumoto Y, Yamamoto K, Suita S *et al.* (2006). MYCN gene amplification is a powerful prognostic factor even in infantile neuroblastoma detected by mass screening. *Br J Cancer* **94**: 1510–1515.

Islam A, Kageyama H, Takada N, Kawamoto T, Takayasu H, Isogai E *et al.* (2000). High expression of Survivin, mapped to 17q25, is significantly associated with poor prognostic factors and promotes cell survival in human neuroblastoma. *Oncogene* **19**: 617–623.

Jain AN, Tokuyasu TA, Snijders AM, Segraves R, Albertson DG, Pinkel D. (2002). Fully automatic quantification of microarray image data. *Genome Res* **12**: 325–332.

Kaneko M, Tsuchida Y, Mugishima H, Ohnuma N, Yamamoto K, Kawa K *et al.* (2002). Intensified chemotherapy increases the survival rates in patients with stage 4 neuroblastoma with MYCN amplification. *J Pediatr Hematol Oncol* **24**: 613–621.

Levy IG. (2005). Neuroblastoma, well-designed evaluations, and the optimality of research funding: ask not what your country can do for you. *J Natl Cancer Inst* **97**: 1105–1106.

Look AT, Hayes FA, Nitschke R, McWilliams NB, Green AA. (1984). Cellular DNA content as a predictor of response to chemotherapy in infants with unresectable neuroblastoma. *N Engl J Med* **311**: 231–235.

Maris JM, Matthay KK. (1999). Molecular biology of neuroblastoma. *J Clin Oncol* **17**: 2264–2279.

Nakagawara A. (1998). The NGF story and neuroblastoma. *Med Pediatr Oncol* **31**: 113–115.

Nakagawara A. (2004). Neural crest development and neuroblastoma: the genetic and biological link. *Prog Brain Res* **146**: 233–242.

Nakagawara A, Arima-Nakagawara M, Scavarda NJ, Azar CG, Cantor AB, Brodeur GM. (1993). Association between high levels of expression of the TRK gene and favorable outcome in human neuroblastoma. *N Engl J Med* **328**: 847–854.

Oba S, Tomioka N, Ohira M, Ishii S. (2006). Combfit: a normalization method for array CGH data. *IPSJ Trans Bioinformatics* **47**: 73–82.

Ohira M, Morohashi A, Inuzuka H, Shishikura T, Kawamoto T, Kageyama H *et al.* (2003). Expression profiling and characterization of 4200 genes cloned from primary neuroblastomas: identification of 305 genes differentially expressed between favorable and unfavorable subsets. *Oncogene* **22**: 5525–5536.

Ohira M, Oba S, Nakamura Y, Isogai E, Kaneko S, Nakagawa A *et al.* (2005). Expression profiling using a tumor-specific cDNA microarray predicts the prognosis of intermediate risk neuroblastomas. *Cancer Cell* **7**: 337–350.

Pinkel D, Segraves R, Sudar D, Clark S, Poole I, Kowbel D *et al.* (1998). High resolution analysis of DNA copy number variation using comparative genomic hybridization to microarrays. *Nat Genet* **20**: 207–211.

Sawada T, Hirayama M, Nakata T, Takeda T, Takasugi N, Mori T *et al.* (1984). Mass screening for neuroblastoma in infants in Japan. Interim report of a mass screening study group. *Lancet* **2**: 271–273.

Schwab M, Westermann F, Hero B, Berthold F. (2003). Neuroblastoma: biology and molecular and chromosomal pathology. *Lancet* **4**: 472–480.

Snijders AM, Nowak N, Segraves R, Blackwood S, Brown N, Conroy J *et al.* (2001). Assembly of microarrays for genome-wide measurement of DNA copy number. *Nat Genet* **29**: 263–264.

Srivatsan ES, Ying KL, Seeger RC. (1993). Deletion of chromosome 11 and of 14q sequences in neuroblastoma. *Genes Chromosomes Cancer* **7**: 32–37.

Storey JD, Tibshirani R. (2003). Statistical significance for genome-wide studies. *Proc Natl Acad Sci USA* **100**: 9440–9445.

Tomioka N, Kobayashi H, Kageyama H, Ohira M, Nakamura Y, Sasaki F *et al.* (2003). Chromosomes that show partial loss or gain in near-diploid tumors coincide with chromosomes that show whole loss or gain in near-triploid tumors: evidence suggesting the involvement of the same genes in the tumorigenesis of high- and low-risk neuroblastomas. *Genes Chromosomes Cancer* **36**: 139–150.

Tonini GP. (1993). Neuroblastoma: the result of multistep transformation? *Stem Cells* **11**: 276–282.

Vandesompele J, Van Roy N, Van Gele M, Laureys G, Ambros P, Heimann P *et al.* (1998). Genetic heterogeneity of neuroblastoma studied by comparative genomic hybridization. *Genes Chromosomes Cancer* **23**: 141–152.

Wei JS, Greer BT, Westermann F, Steinberg SM, Son CG, Chen QR *et al.* (2004). Prediction of clinical outcome using gene expression profiling and artificial neural networks for patients with neuroblastoma. *Cancer Res* **64**: 6883–6891.

White PS, Maris JM, Beltinger C, Sulman E, Marshall HN, Fujimori M *et al.* (1995). A region of consistent deletion in neuroblastoma maps within human chromosome 1p36.2–36.3. *Proc Natl Acad Sci USA* **92**: 5520–5524.

Woods WG, Gao RN, Shuster JJ, Robison LL, Bernstein M, Weitzman S *et al.* (2002). Screening of infants and mortality due to neuroblastoma. *N Engl J Med* **346**: 1041–1046.

Supplementary Information accompanies the paper on the Oncogene web site (http://www.nature.com/onc).

Oncogene (2008) 27, 741–754

www.nature.com/onc

ORIGINAL ARTICLE

Stress via p53 pathway causes apoptosis by mitochondrial Noxa upregulation in doxorubicin-treated neuroblastoma cells

K Kurata[1], R Yanagisawa[1], M Ohira[2], M Kitagawa[3], A Nakagawara[2] and T Kamijo[1,2]

[1]Department of Pediatrics, Shinshu University School of Medicine, Matsumoto, Nagano, Japan; [2]Division of Biochemistry, Chiba Cancer Center Research Institute, Chuoh-ku, Chiba, Japan and [3]Department of Biochemistry, Hamamatsu University School of Medicine, Hamamatsu, Shizuoka, Japan

In this study, we employed a panel of cell lines to determine whether p53-dependent cell death in neuroblastoma (NB) cells is caused by apoptotic cellular function, and we further studied the molecular mechanism of apoptosis induced via the p53-dependent pathway. We obtained evidence that a type of p53-dependent stress, doxorubicin (Doxo) administration, causes accumulation of p53 in the nucleus of NB cells and phosphorylation of several serine residues in both Doxo-sensitive and -resistant cell lines. Upregulation of p53-downstream molecules in cells and upregulation of Noxa in the mitochondrial fraction were observed only in Doxo-sensitive NB cells. Significance of Noxa in the Doxo-induced NB cell death was confirmed by Noxa-knockdown experiments. Mitochondrial dysfunction, including cytochrome-*c* release and membrane potential disregulation, occurred and resulted in the activation of the intrinsic caspase pathway. However, in the Doxo-resistant cells, the accumulation in the nucleus and phosphorylation of p53 did not induce p53-downstream $p21^{Cip1/Waf1}$ expression and the Noxa upregulation, resulting in the retention of the mitochondrial homeostasis. Taken together, these findings indicate that the p53 pathway seems to play a crucial role in NB cell death by Noxa regulation in mitochondria, and inhibition of the induction of p53-downstream effectors may regulate drug resistance of NB cells.

Oncogene (2008) **27**, 741–754; doi:10.1038/sj.onc.1210672; published online 20 August 2007

Keywords: neuroblastoma; p53; noxa; mitochondria; apoptosis

Introduction

Neuroblastoma (NB) is the most common pediatric solid malignant tumor derived from the sympathetic nervous system. Unlike the many childhood malignancies for which survival has been improved by recent therapies, high-risk NB is still one of the most difficult tumors to cure, with only 30% long-term survival despite intensive multimodal therapy. New treatments and a better understanding of drug resistance mechanisms are required for the improvement of the survival rate. A noteworthy finding of NB research is that mutations of p53 tumor suppressor have been reported in less than 2% of NBs out of 340 tested (Tweddle *et al.*, 2001). Instead of mutation, cytoplasmic sequestration of p53 has been proposed as an alternative mechanism of inactivation in NB cells. The sequestration was first detected in frozen tumor samples using immunohistochemical techniques (Moll *et al.*, 1995) and later in NB cell lines by immunofluorescence and cell fractionation experiments (Moll *et al.*, 1996). However, several groups reported nuclear p53 accumulation in NB cells harboring wild-type p53 after DNA damage (Tweddle *et al.*, 2003). After nuclear accumulation, p53 phosphorylation, binding to targeted sequences and transcriptional transactivation are sequentially induced by DNA damage in *p53* wild-type cells (Oren, 1999). However, these processes in NB cells harboring wild-type p53 have not been examined with respect to the role of p53 pathways in the tumorigenesis of NB. Their examination should also yield insights into the molecular mechanisms of p53 inactivation. For instance, upregulation of the p53-downstream genes encoding $p21^{Cip1/Waf1}$ and HDM2 in *p53* wild-type NB cell lines was observed in several studies (Isaacs *et al.*, 2001; Keshelava *et al.*, 2001; Tweddle *et al.*, 2001) but not all (Wolff *et al.*, 2001). Reporter gene assays detected p53 transcriptional function in one study (Keshelava *et al.*, 2001) but not in another (Wolff *et al.*, 2001). Together, these facts indicate that systematic and detailed analysis of the biological effects of p53-dependent stress on the cell death of NB cells and of the mechanisms of activation and signal transduction of p53-related pathways in NB cells are required for understanding the mechanism of drug resistance and for the development of new therapies for high-risk NB patients.

The Bcl-2 family member proteins regulate mitochondrial cell death by controlling mitochondrial outer membrane permeabilization (MOMP). Anti-apoptotic Bcl-2 family members (for example, Bcl-2, Bcl-xL, Bcl-w and Mcl-1) function to block MOMP, whereas the

Correspondence: Dr T Kamijo, Division of Biochemistry, Chiba Cancer Center Research Institute, 666-2 Nitona, Chuoh-ku, Chiba 260-8717, Japan.
E-mail: tkamijo@chiba-cc.jp
Received 4 December 2006; revised 1 June 2007; accepted 11 June 2007; published online 20 August 2007

various pro-apoptotic proteins promote it. The pro-apoptotic proteins fall into two general subfamilies, based on the sharing of Bcl-2 homology domains. BH123 proteins appear to be effectors of MOMP, because cells from mice lacking the two major BH123 proteins, Bax and Bak, fail to undergo MOMP in response to a wide range of apoptotic stresses (Wei *et al*., 2001). The other subfamily, the BH3-only proteins, can act either to activate Bax or Bak or to interfere with the anti-apoptotic Bcl-2 family members (Letai *et al*., 2002). Noxa is a BH3-only member of Bcl-2 family proteins (Oda *et al*., 2003) and its expression is induced by DNA damage such as that caused by etoposide or doxorubicin in a p53-dependent manner (Oda *et al*., 2003; Shibue *et al*., 2003). Furthermore, several lines of evidence reported that Noxa is one of the most important cell death effectors in neuronal cell death, for example, nuclear factor-kappa B modulated cell death in mouse cortical neurons (Aleyasin *et al*., 2004), axotomized motor neurons of adult mouse (Kiryu-Seo *et al*., 2005), sensory neurons especially in trigeminal ganglia and cervical dorsal ganglia (Hudson *et al*., 2005) and arsenite-induced cortical neurons (Wong *et al*., 2005).

These results have led us to study the role and molecular machinery of p53-dependent cell death in NB by utilizing several *p53* wild-type NB cell lines. We studied the sensitivities of NB cell lines to doxorubicin (Doxo), which is a representative cytotoxic drug against NB cells (Matthay *et al*., 1998) that induces stresses that are basically dependent on p53 (Lowe *et al*., 1994), and transactivates p53 and its downstream effectors in many tissues (Komarova *et al*., 1997). In sensitive NB cells, the following important findings were observed after Doxo treatment: (1) accumulation of p53 in the nucleus; (2) activation of the p53-downstream molecules; (3) pro-apoptotic BH3-only Bcl-2 family protein Noxa induction and upregulation in mitochondria resulting in mitochondrial dysfunction/intrinsic caspase-derived apoptosis. Although p53 accumulated in the nucleus before Doxo treatment, the downstream molecules were not induced and the upregulation of Noxa in mitochondria was not observed in the Doxo-resistant NB cells. Consequently, the crucial role of the p53 pathway in apoptosis in NB cells was indicated by our observations.

Results

Heterogeneity of response to p53-dependent death signals in NB cell lines harboring wild-type p53

We chose 0.5 μg/ml of Doxo as an appropriate concentration to assess the effect of Doxo on NB cells according to the results of the analysis of peak plasma concentrations of doxorubicin (Hempel *et al*., 2002). Similar results were obtained by 0.3–1.0 μg/ml of Doxo in the following experiments (data not shown). Trypan blue uptake assays were performed to compare the Doxo sensitivity of NB cell lines harboring wild-type *p53* (Figure 1a). More than 60% of cells were Trypan blue-positive for the SH-SY5Y, NB9, NB69 and SK-N-SH NB cell lines 36 h after Doxo stimulation. On the other hand, less than 40% of cells were positive in NB-19 and NB1 cell lines and less than 10% in IMR32 cells even 36 h after Doxo stimulation.

Next, we performed WST-8 assay, a modification of MTT assay, to evaluate cytotoxicity on NB cells (Figure 1b). We confirmed the sensitivity of NB cells to Doxo by these experiments and also studied the effects of etoposide, the other p53-dependent damage-inducing reagent, on NB cells. Etoposide was effectively cytotoxic on the Doxo-sensitive SK-N-SH, SH-SY5Y, NB-9 and NB-69 cells. In the Doxo-resistant NB cells, IMR32 and NB-1 cells also possessed drug resistance against etoposide, whereas NB-19 cells had sensitivity.

FACS analysis of sub-G_0/G_1 cells showed that considerable percentages of cells underwent apoptosis 24 h after the Doxo treatment in SH-SY5Y, NB-9, NB-69 and SK-N-SH (Figure 1c). However, the proportions of apoptotic cells were significantly lower in NB-19, NB-1 and IMR32 than in the four Doxo-sensitive NB cell lines. In SK-N-SH and SH-SY5Y cells, the increase of the sub-G_0/G_1 fraction after Doxo treatment was confirmed by the condensation and fragmentation of nuclei (Figure 1d). In contrast, almost all of the nuclei were intact in the resistant IMR32 and NB-1 cells. Thus, Doxo-induced stresses resulted in apoptosis in some NB cells, whereas others were resistant (Figure 1).

Upregulation and nuclear accumulation of p53 are not enough to induce apoptosis by Doxo treatment

To study the basis of the different sensitivities of NB cells to p53-dependent stress, we first performed direct western blot analysis using a monoclonal antibody recognizing the p53 N terminus (DO1) to estimate the total amount of p53. We also used antibodies that specifically react with phosphorylated serine residues (Ser15, Ser20 and Ser46) to examine the modulation of the stability and/or activity of p53 in response to DNA damage.

The amount of p53 was clearly increased by Doxo in the Doxo-sensitive NB cells, as detected with DO1 antibody (Figure 2a). p53 accumulation was observed in the Doxo-resistant IMR32 and NB-19 cells before treatment; serine15 phosphorylation was induced in all the NB cells after Doxo exposure. Upregulation of serine46 phosphorylation was also observed in the NB cell lines, except for IMR32 and SH-SY5Y cells. On the other hand, ser20 phosphorylation was not strongly upregulated in any of the lines. Consistent with previous reports, RT–PCR analysis showed that the induction of p53 protein by Doxo treatment in sensitive-NB cells was not caused at the transcriptional level (Figure 2b). Thus, it appears that the upregulation of p53 protein in Doxo-treated NB cells seemed to be caused by protein stabilization.

Next, we investigated the localization of p53 in NB cells, using DO1 as a human p53-specific antibody reacting with amino acids 21–25, pAb421 as a pan-p53 antibody reacting with the human p53 amino acids 370–378 and

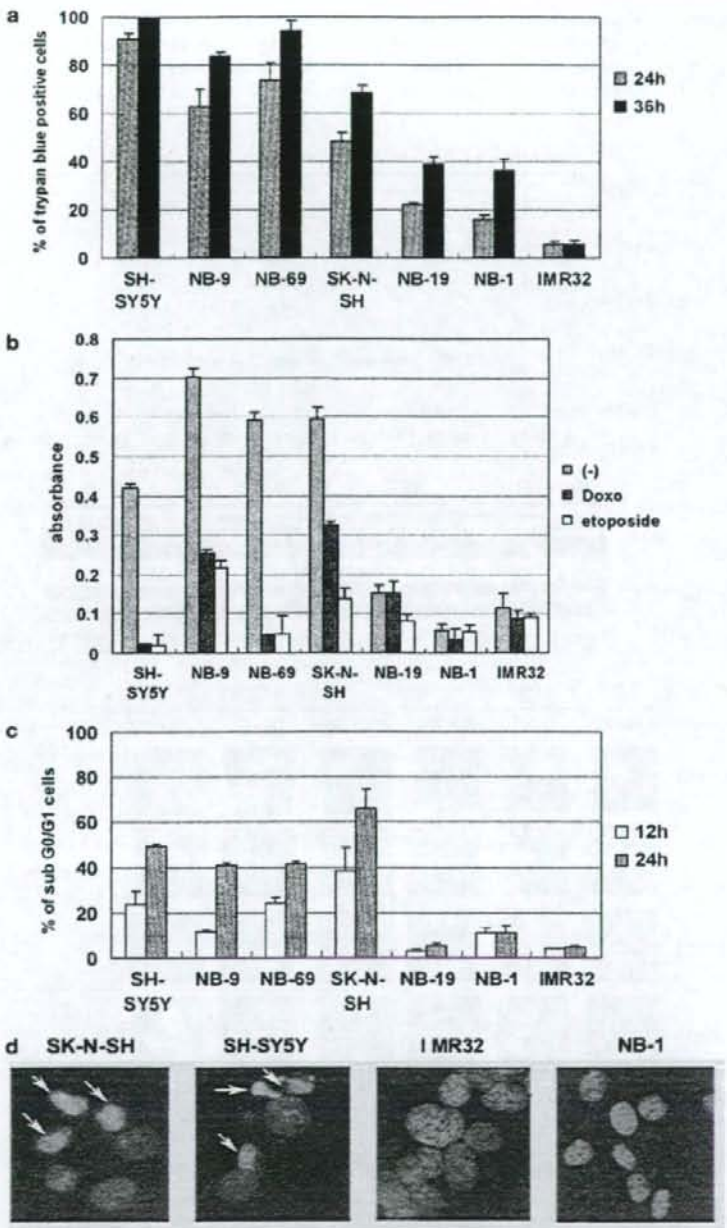

Figure 1 Sensitivity to doxorubicin (Doxo) is heterogenic in wild-type p53 harboring neuroblastoma (NB) cells. One hundred thousand cells were plated in a 3-cm-diameter culture dish and cultured in 5% CO_2 for 24 h. Doxo was added to the dish at 0.5 μg/ml and the incubation was continued for the indicated times. Mean and standard deviation (s.d.) of the % of cells were calculated for triplicate samples. (**a**) Cells were washed with 1 × phosphate-buffered saline (PBS), collected by 1 × PBS/0.5 mM EDTA, and stained with Trypan blue. The results are representative of four independent experiments. (**b**) After treatment of DNA-damaging reagents, cell viabilities were analysed by WST-8 assay. The results are representative of at least three independent experiments. (**c**) Analysis of the sub-G_0/G_1 fraction was performed as described in Materials and methods. The results are representative of three independent experiments. (**d**) Staining with 4′,6-diamidino-2-phenylindole (DAPI) was performed 24 h after Doxo stimulation. Arrows indicate the condensed or fragmented nuclei.

16G8 as an anti-phosphorylated p53ser15 antibody. Staining with pAb421 antibody revealed that the punctate cytoplasmic signal was upregulated in both Doxo-sensitive and -resistant NB cells after Doxo exposure (Figure 2c). DO1 antibody showed both nuclear and cytoplasmic staining before treatment, and remarkable accumulation into the nucleus was induced by Doxo in these four NB cell lines. Although ser15 phosphorylation was hardly

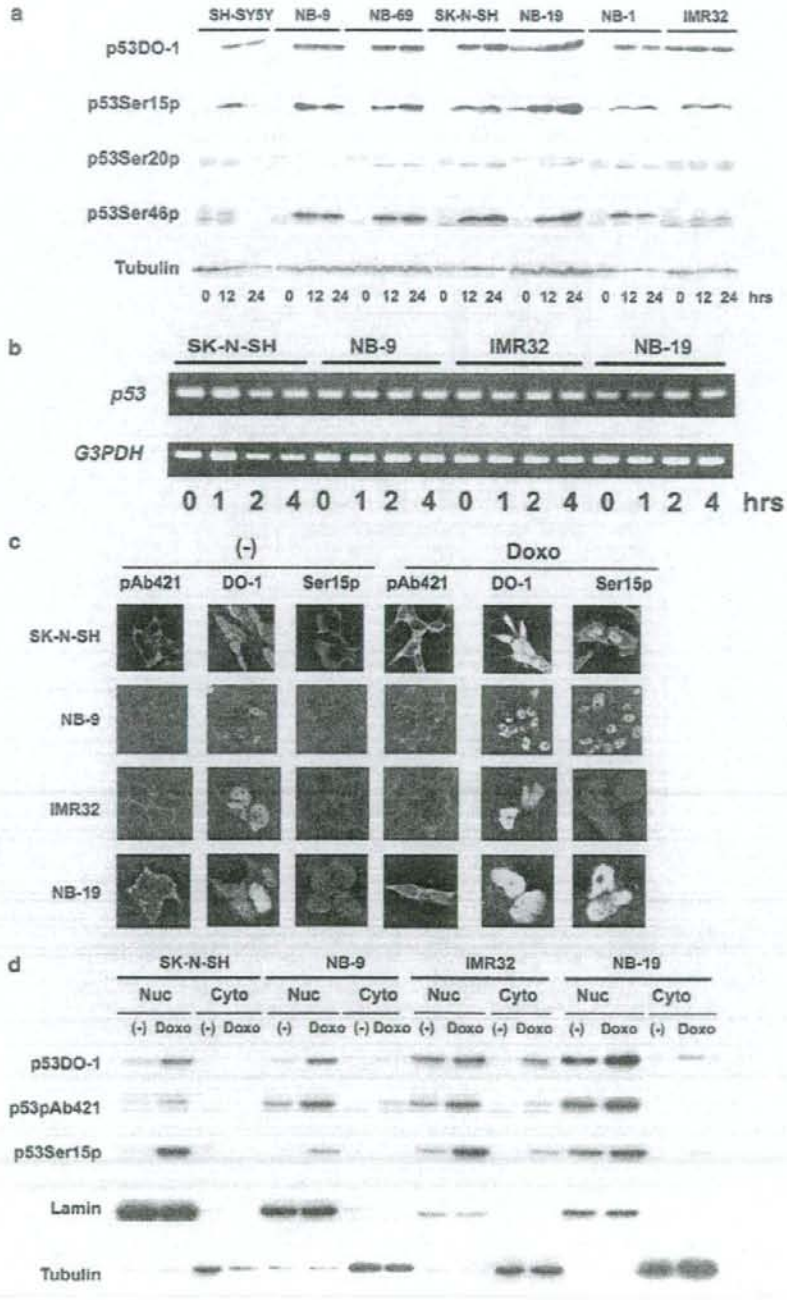

detected before treatment, the phosphorylation was remarkably upregulated by Doxo in SK-N-SH, NB-9 and NB-19 cells. In IMR32 cells, p53ser15 phosphorylation was modestly upregulated. The ser15-phosphorylated p53 accumulated to a much greater degree in the nucleus than in the cytoplasm after Doxo treatment. The use of several different fixation methods and modification of the first antibody concentration did not influence the results of immunofluorescence. Moreover, *p53* wild-type MCF7 cells showed similar staining results with these antibodies (data not shown). To investigate the observed discrepancy of p53 localization among the three monoclonal antibodies in the immunofluorescence experiments, we performed cell fractionation experiments (Figure 2d). All of the p53 signals were detected only in the nucleus before the treatment, and the upregulated signals induced by Doxo also accumulated in the nucleus rather than in the cytoplasm. The controls for fractionation, the nuclear marker lamin and cytoplasmic marker β-tubulin, were detected in the proper fractions and the amounts were not changed by Doxo treatment. These results show that the p53-dependent Doxo-stress increased the amount of p53 and induced the accumulation of p53 in the nucleus in both Doxo-sensitive and -resistant NB cells.

Activity of p53 as a transcriptional factor is required for Doxo-induced NB apoptosis

We then assessed the induction of p53-downstream molecules by Doxo. As shown in Figure 3a, exposure to Doxo induced remarkable $p21^{Cip1/Waf1}$ protein accumulation in the sensitive cells but not in the resistant cells, and this induction was caused at the transcriptional level (Figure 3b). HDM2 was similarly induced by Doxo treatment in the sensitive cells. However, *HDM2* mRNA accumulated in the resistant cells before Doxo treatment and did not change subsequently (Figure 3b), which is consistent with its protein accumulation (Figure 3a). These results indicate that the Doxo-induced cellular stress can effectively induce the p53 transcriptional activities in Doxo-sensitive NB cells but not in the resistant cells.

Doxo treatment induces synthesis of pro-apoptotic Noxa in the sensitive NB cells but not in the resistant cells

Next, we studied the expression of Bcl-2 family proteins in the NB cells, because regulation of the Bcl-2 family proteins by p53 is known to be the main component of p53-dependent apoptosis (Shen and White, 2001). The pro-apoptotic Bcl-2 family proteins Bax, Bak and Bok were not modified by Doxo in the NB cells (Figure 3a). Expression of Puma and p53AIP1 was also not affected by Doxo treatment (data not shown). It is interesting that Noxa was substantially induced only in the sensitive cells but not in the resistant cells. Although there was a considerable difference in the amount of anti-apoptotic Bcl-2 among the NB cells, its expression seemed not to be related to the Doxo sensitivity. The other anti-apoptotic Bcl-2 family protein Bcl-xL was not detected in any of the NB cells (data not shown). To assess whether the induction of Noxa is regulated at the transcriptional level, we performed semi-quantitative RT–PCR analysis. Consistent with the results of the western blot analysis, the mRNA amount of Noxa was clearly upregulated by Doxo treatment in the Doxo-sensitive SK-N-SH cells (Figure 3b). Meanwhile, the accumulation of *Noxa* mRNA expression was detected in the resistant cells (Figure 3b) and confirmed by quantitative real-time PCR analysis (Figure 3c). However, *Noxa* mRNA was not increased by Doxo treatment in the resistant cells (Figure 3b).

Noxa accumulation in mitochondria is not sufficient to induce apoptosis in NB cells

A recent report demonstrated that Noxa and Bok were induced by DNA stress dependent upon the p53 pathway in the SH-SY5Y cell line (Yakovlev *et al.*, 2004). However, only Noxa upregulation was detected in the present study in the sensitive NB cell lines. Interestingly, larger amounts of Noxa were observed in the Doxo-resistant NB lines (IMR32 and NB-19) compared with the sensitive lines (SK-N-SH and NB-9). Since the organelle-specific amounts of the pro-apoptotic Bcl-2 family protein and its ratio to anti-apoptotic Bcl-2 family proteins in mitochondria are reported to determine cell fate in mitochondria-dependent apoptosis (Nakazawa *et al.*, 2003; Danial and Korsmeyer, 2004), we studied the amounts of Noxa in mitochondria by cell fractionation/western blot analysis (Figure 4A). The amounts of Noxa in mitochondria were apparently upregulated in the sensitive cells. Densitometric analysis revealed that the Doxo-treatment increased the content of Noxa 10.3-fold in SK-N-SH cells and 16.6-fold in NB-9 cells compared to that before stimulation. On the other hand, Noxa was accumulated at higher levels in mitochondria of the resistant cells compared with the sensitive cells before Doxo treatment, and was not further increased by Doxo treatment. There were no significant differences in the amounts of Bcl-2 in the presence or absence of Doxo

Figure 2 Upregulation and nuclear accumulation of p53 in neuroblastoma (NB) cells. (**a**) Cells were collected after Doxo stimulation at the indicated time points (0, 12 and 24 h) and analysed by western blotting with the indicated antibodies (DO-1, p53ser15p, p53ser20p, p53ser46p and β-tubulin) as described in Materials and methods. (**b**) Cells were collected after Doxo stimulation at the indicated time points (0, 1, 2 and 4 h); p53 and G3PDH mRNA expression was analysed by RT PCR as described in the Materials and methods section. (**c**) Cells were analysed by immunofluorescence with the indicated antibodies (pAb421, DO-1 and monoclonal anti-p53ser15p antibody: 16G8) 12 h after Doxo stimulation. (**d**) Cells were collected 12 h after Doxo stimulation and subjected to cell fractionation experiments as described in Materials and methods. Twenty micrograms of the proteins extracted from the organelle was analysed by sodium dodecyl sulfate polyacrylamide gel electrophoresis (SDS PAGE)/western blot experiments using the indicated antibodies. Lamin was used as a positive control for nuclear localization, and β-tubulin for cytosolic localization.

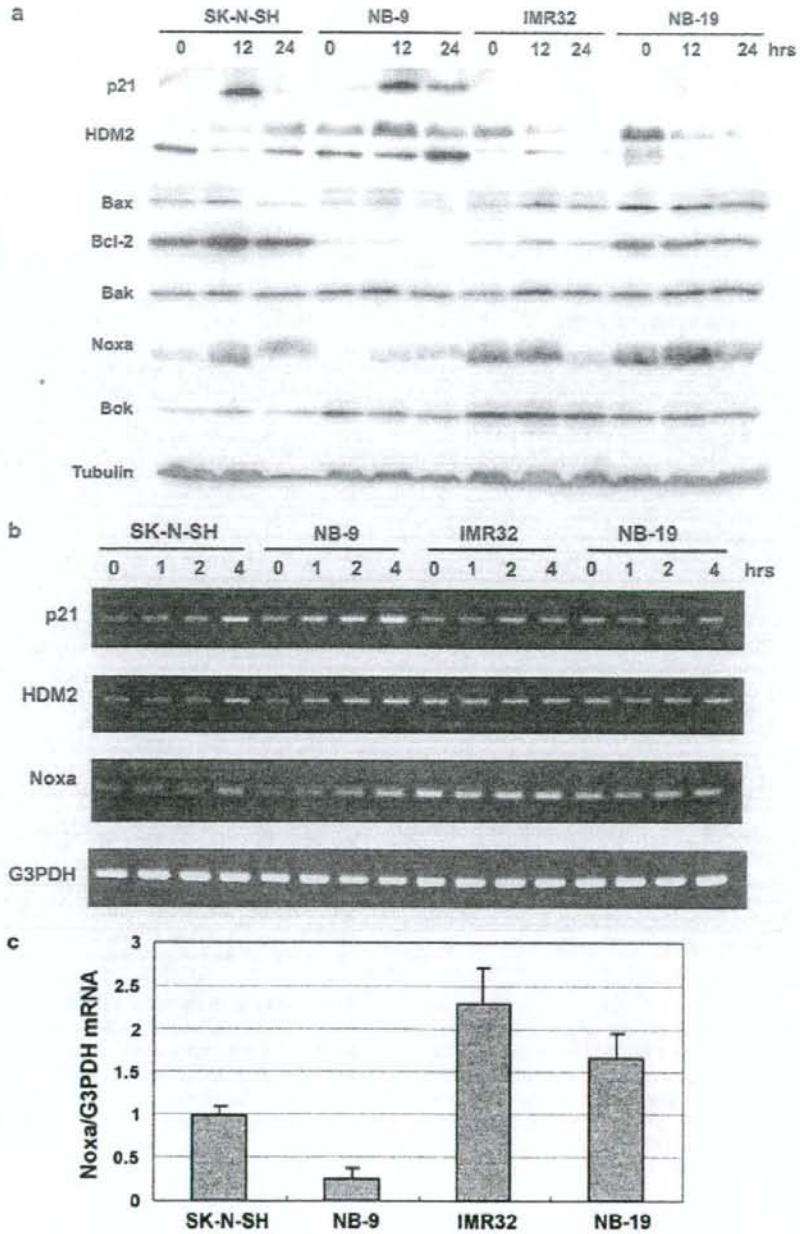

Figure 3 Modulation of p53-downstream proteins by Doxo treatment. The neuroblastoma (NB) cells were incubated with or without Doxo and collected at the indicated time points. (**a**) Extracted total cell lysates were subjected to sodium dodecyl sulfate polyacrylamide gel electrophoresis (SDS PAGE)/western blot analysis using the antibodies against the indicated molecules as described in Materials and methods. (**b**) Total RNA was subjected to semi-quantitative RT PCR analysis as described in the Materials and methods section. (**c**) Quantitative real-time PCR analysis of *Noxa* mRNA amounts in NB cells as described in the methods section. Total RNA was extracted from unstimulated NB cells.

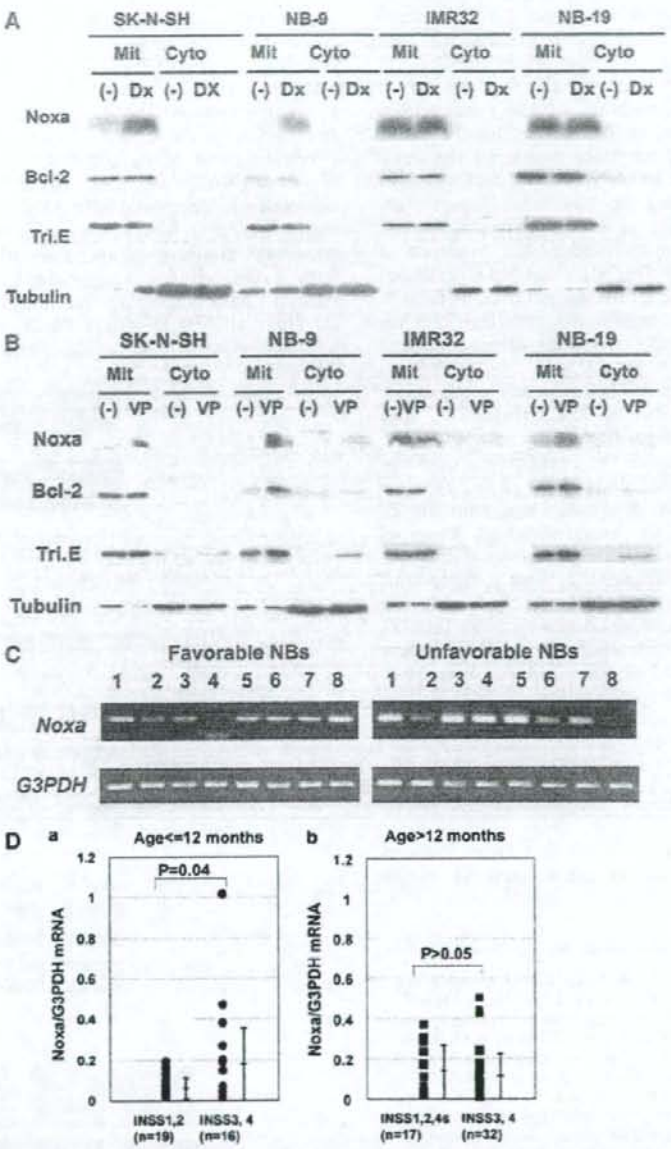

Figure 4 Noxa is upregulated in mitochondria by Doxo in the sensitive neuroblastoma (NB) cells. (**A** and **B**) Cells were collected 12 h after stimulation by Doxo (A, DX) or etoposide (B, VP) and subjected to cell fractionation for mitochondria (heavy membrane fraction: Mit) and the light membrane/cytosol fraction (Cyto). Samples were analysed by sodium dodecyl sulfate polyacrylamide gel electrophoresis (SDS PAGE)/western blotting with the indicated antibodies. Trifunctional protein (Tri E) and tubulin were controls for the mitochondrial fraction and cytosolic/light membrane fraction, respectively. This is a representative result of three independent experiments. (**C**) Semi-quantitative RT PCR analysis of Noxa mRNA in favorable (stage 1 or 2, with single copy *MYCN*) and unfavorable (stage 3 or 4, with *MYCN* amplification) NB samples. (**D**) Quantitative real-time RT PCR analysis of *Noxa* mRNA in 84 tumor samples from patients with NBs according to the tumor stage. The levels of Noxa were normalized to that of G3PDH. Results are presented as closed circles (**Da**) and closed squares (**Db**) with mean ± s.d. bars.

between the sensitive and resistant cells. Bcl-xL was not detected even by the fractionation experiments (not shown). The localization of trifunctional protein in mitochondria (Kamijo *et al*., 1993) and β-tubulin in the cytosol confirmed the reliability of the fractionation procedures. Importantly, similar results on the Noxa kinetics in mitochondria were observed after the treatment by etoposide, the other p53-dependent damage-inducing anticancer drug in NB cells (Figure 4B). Consistent with the results of WST-8 assay (Figure 1b), Noxa upregulation in mitochondria was observed in etoposide-sensitive SK-N-SH, NB-9 and NB-19 cells but not in IMR32 cells. These results suggest that the ratio of pro- to anti-apoptotic molecules such as Noxa/Bcl-2 has a strong impact on the p53-dependent damage-induced apoptosis in NB cells.

Next, we assessed *Noxa* mRNA amounts in NB tumor samples by semi-quantitative RT–PCR (Figure 4C) and quantitative real-time reverse transcriptional (RT)–PCR (Figure 4D). Consistent with the upregulation of *Noxa* mRNA in the resistant cell lines (Figures 3b and c), some unfavorable NB samples expressed large amounts of *Noxa* mRNA (Figure 4C). Especially, high levels of *Noxa* mRNA expression were significantly associated with INSS3 and INSS4 samples that were younger than 12 months old ($P=0.04$) according to the Welch test (Figure 4D). In the NB samples that were older than 12 months old, no obvious difference was detected, mainly due to the high expression of Noxa in INSS 1 samples. Although we checked the correlation of *MYCN* and *Noxa* mRNA expression, there was no significant correlation (data not shown).

Knockdown of Noxa effectively reduces Doxo-induced cell death in NB cells

To definitively establish a role of Noxa in Doxo-induced cell death in NB cells, both of the sensitive SK-N-SH cells and the resistant IMR32 cells were treated with *Noxa* small interfering RNA (siRNA) and then the NB cells had Doxo administered. Preincubation of the NB cells with the *Noxa* siRNA but not control siRNA effectively reduced the *Noxa* mRNA and also protein amounts in SK-N-SH cells (Figures 5a and b). Since the effectiveness of *Noxa* siRNA1 is better than that of *Noxa* siRNA2, we used *Noxa* siRNA1 for later experiments. The *Noxa* siRNA1 did not affect the pro-apoptotic Bcl-2 family molecules (Bax and Bak), an important inhibitor of apoptosis $p21^{Cip1/Waf1}$ and interferon-α (Figure 5c), suggesting that the knockdown seems to have a specific effect on Noxa. The ability of the *Noxa* siRNA to reduce the *Noxa* mRNA amounts was accompanied by a significant reduction in the

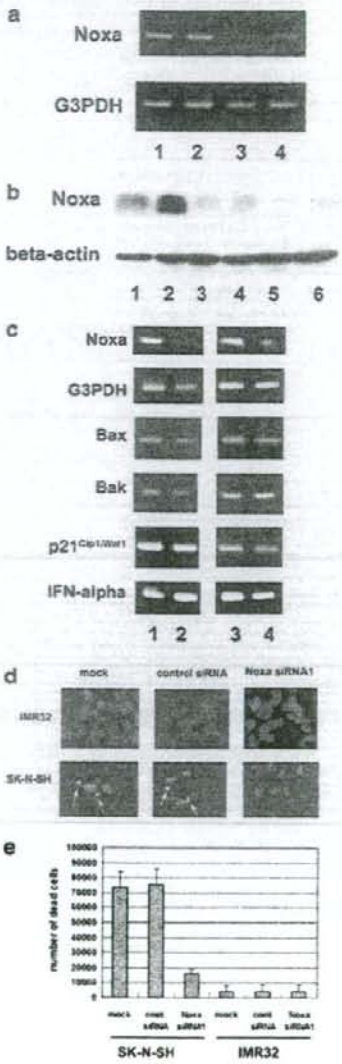

Figure 5 Noxa knockdown cancels Doxo-induced apoptotic cell death in sensitive neuroblastoma (NB) cells. (**a**) SK-N-SH cells were collected 48 h after small interfering RNA (siRNA) treatment (lane 1: mock; lane 2: control siRNA; lane 3: Noxa siRNA1; lane 4: Noxa siRNA2) and subjected to cDNA synthesis/semi-quantitative RT PCR procedure. (**b**) SK-N-SH cells (lane 3: mock; lane 4: control siRNA; lane 5: Noxa siRNA1; lane 6: Noxa siRNA2) were collected 48 h after siRNA treatment and 30 μg of proteins was subjected to sodium dodecyl sulfate polyacrylamide gel electrophoresis (SDS PAGE)/western blot analysis. Lanes 1 and 2 were nontreated IMR32 and NB-19 cells, respectively, as controls. (**c**) Forty-eight hours after the siRNA treatment, cells were treated with 0.5 μg/ml Doxo. Twenty-four hours after Doxo administration, SK-N-SH (lanes 1 and 2) and IMR32 (lanes 3 and 4) cells were collected and subjected to cDNA synthesis/semi-quantitative RT PCR for the analysis of the molecules indicated at the left side of panel. Lanes 1 and 3 are control siRNA treated, and lanes 2 and 4 are Noxa siRNA1 treated. (**d** and **e**) Forty-eight hours after the siRNA treatment, cells were treated with 0.5 μg/ml Doxo. Twenty-four hours after Doxo administration, the culture dish-attached SK-N-SH and IMR32 cells were stained with 4′,6-diamidino-2-phenylindole (DAPI) and nuclear morphology was analysed. The floating cells were collected and subjected to Trypan blue uptake analysis. Trypan blue-positive cells were counted as 'dead cells.'

apoptotic morphological change of nuclei (nuclear condensation and fragmentation, Figure 5c) and cell death (Figure 5d) in the Doxo-sensitive SK-N-SH cells but not in the resistant IMR32 cells.

Doxo-induced stress induces mitochondrial dysfunction and activates the intrinsic caspase pathway

Next, we evaluated mitochondria homeostasis and activation of caspase pathways in NB cells. First, we investigated the role of mitochondrial membrane potential in Doxo-induced apoptosis. Mitochondrial membrane potential was assessed 10 h after Doxo stimulation by staining with the mitochondrion-selective dye, MitoTracker. Doxo-sensitive cells exhibited substantial mitochondrial depolarization, as evidenced by the loss of MitoTracker staining (Figure 6a). In contrast, depolarization was not induced by Doxo in the resistant cells. Next, immunofluorescence experiments showed that cytochrome-*c* was clearly released from mitochondria in the sensitive cells but not in the resistant cells (Figure 6b, Doxo-treated cells, 'Cyto. C' panels). Nuclear condensation was especially observed in the cells from which large amounts of cytochrome-*c* were released (Doxo-treated cells, 'Nuc' panels). These results suggest that mitochondrial dysfunction plays a pivotal role in Doxo-induced apoptosis in NB cells.

The central component of apoptosis is a proteolytic system involving a family of proteases called caspases (Green, 2000). As shown in Figure 6c, pro-caspase-9 cleavage was observed in the Doxo-sensitive cells, but not in the resistant cells 12 h after exposure to Doxo. The substrates of the activated caspase-9, pro-caspase-3 and -7 were also cleaved in the Doxo-sensitive cells. These findings suggest that apoptotic signals induced by Doxo activate the intrinsic caspase pathway via a mitochondrial pathway in NB cells, resulting in cell death of the Doxo-sensitive NB cells. Meanwhile, the resistant cells showed no activation of these initiator (caspase-9) and effector (caspase-3 and/or -7) caspases.

Discussion

Human *Noxa* is located on chromosome 18q21 and its promoter region contains a p53-responsive element (Oda *et al*., 2003). The expression of p53 increases human *Noxa* mRNA, and ectopic expression of Noxa effectively induces apoptosis in a BH3-motif-dependent manner (Oda *et al*., 2003). In the present study, we observed that Doxo-sensitive NB cells exhibited the Noxa mRNA/protein induction and protein localization into mitochondria after the treatment with Doxo, leading to an increase in the ratio of pro-/anti-apoptotic Bcl-2 family proteins. Mitochondrial dysfunction and intrinsic caspase-mediated apoptosis were also induced in the sensitive cells. Notably, apoptosis was almost completely canceled by the knockdown of Noxa by siRNA, confirming the importance of Noxa in the Doxo-induced apoptosis of NB cells. Taken together, these findings indicate that the Noxa upregulation in mitochondria may play an important role in Doxo-induced apoptosis in NB cells. A previous study described that Noxa and Bok were induced by etoposide, and *Noxa* siRNA treatment reduced etoposide-induced cell death in SH-SY5Y NB cells (Yakovlev *et al*., 2004). Furthermore, Obexer *et al*. (2007) reported that Noxa and Bim are effectors of FKHRL-1-induced apoptosis in NB cells. Since we also observed the upregulation of Noxa in mitochondria by Doxo or etoposide treatment, Noxa seems to be one of the important effectors of the pro-apoptotic signaling pathway in NB cell apoptosis.

Whereas Yakovlev *et al*. (2004) did not use stress-resistant NB cells, the kinetics of Noxa induction in the stress-resistant NB cells was evaluated in our study. In the Doxo-resistant NB cells, exposure to Doxo failed to increase the expression of Noxa and the other downstream molecules in mitochondria, although p53 was abundant in the nucleus before Doxo exposure and some of the p53 serine residues that regulate p53 stability and activity (Shieh *et al*., 1997; Oda *et al*., 2000) were efficiently phosphorylated in the resistant cells, as well as in the sensitive cells. These results suggest that the lack of some p53 function in the resistant NB cells results in the failure of apoptosis, even under the pressure of DNA damage, such as Doxo treatment. It is of interest that the amounts of *Noxa* mRNA and protein in the mitochondria were much larger in the unstimulated resistant cells than in the sensitive cells but not stimulated by Doxo treatment. Alternatively, the inability to upregulate Noxa transcription in response to Doxo may be related to resistance to the anthracycline in some NB cells. Large amounts of *Noxa* mRNA in a part of unfavorable NB primary tumor samples (Figure 4C) supported the observation of inactivity of accumulated Noxa in the resistant cells. The accumulation of Noxa in unstimulated NB cells seems to be p53 independent, as it was suggested by our experiments. Although several findings suggest that Noxa is induced via a p53-independent pathway in neuronal cells (Kiryu-Seo *et al*., 2005; Wong *et al*., 2005), the exact molecular pathway responsible for the p53-independent Noxa induction in NB remains to be elucidated. One possibility is the presence of other p53 family proteins, for example, p63 and p73 proteins in NB cells. Actually, p73-alpha is expressed in several NB cell lines, including IMR32 and NB19 cells, and p63, but not deltaNp63, is highly expressed at the transcriptional level in IMR32 cells (data not shown). The study of the physiological role of p63 and p73 proteins on Noxa expression and Doxo-induced NB cell death seems to be meaningful for research of NB cell death.

A previous report indicated that although Noxa expression mediated by adenovirus could not induce apoptosis in either wild-type or *p53*-knockout MEFs, its expression effectively enhanced the apoptotic response to etoposide or UV (Shibue *et al*., 2003), suggesting that Noxa induces apoptosis in concert with not only p53-dependent cellular signals, but also p53-independent cellular signals. Additionally, we found a significant increase of *Noxa* mRNA amounts in the tumor samples

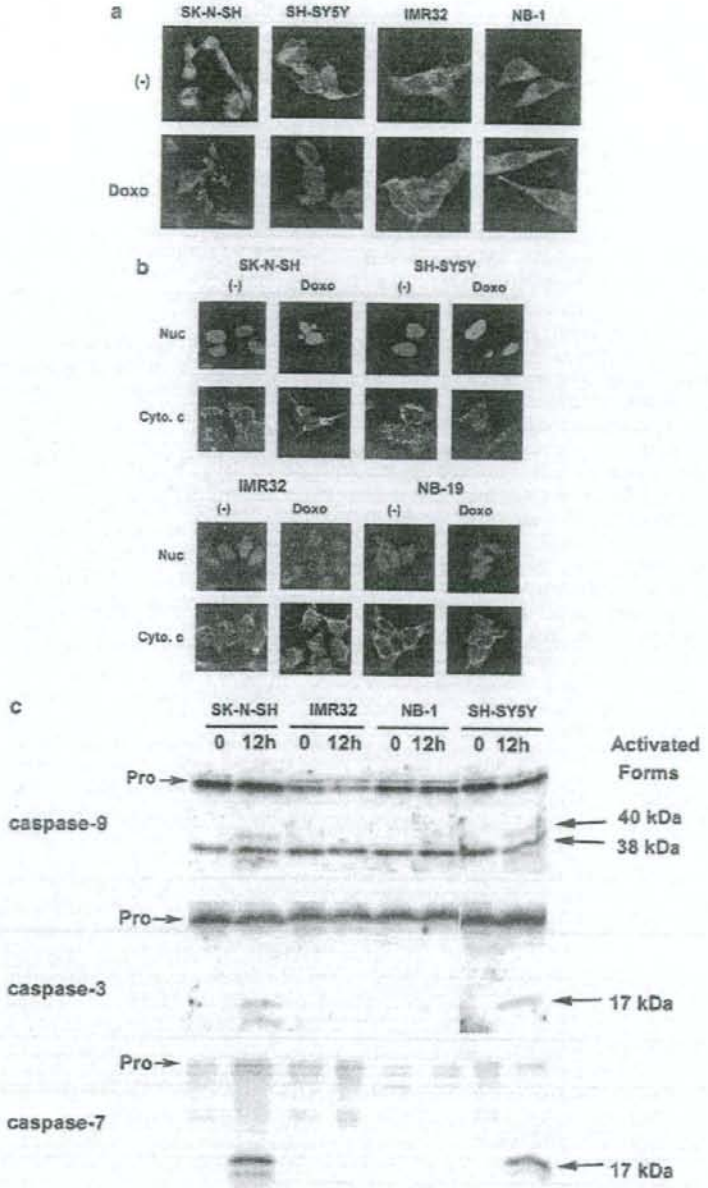

Figure 6 Mitochondrial dysfunction is induced by Doxo in the sensitive neuroblastoma (NB) cells. (**a**) Mitochondrial membrane potential was detected using MitoTracker dye 6 h after Doxo stimulation (Doxo). The steady-state potential is shown as a control [(−)]. (**b**) Cells were stimulated with Doxo for 6 h, and then cytochrome-*c* (Cyto. c) signals were detected by immunofluorescence experiments. The nucleus (Nuc) was stained with 4′,6-diamidino-2-phenylindole (DAPI). (**c**) Cells were collected at the indicated time points after Doxo stimulation and subjected to sodium dodecyl sulfate polyacrylamide gel electrophoresis (SDS PAGE)/western blot analysis. Processing of pro-caspase-9 was detected by the presence of 38/40-kDa cleaved forms. The anti-caspase-3 rabbit polyclonal antibody (BD Pharmingen) recognized the 32-kDa pro-caspase-3 and the 17-kDa cleaved form. The anti-caspase-7 mouse monoclonal antibody (clone B94-1) recognized the 35-kDa pro-caspase-7 and the 17-kDa cleaved form.

in the advanced stage (INSS3 and -4, younger than 12 months old) by quantitative real-time RT–PCR analysis (Figure 4D), indicating that the inactiveness of *Noxa* may relate to the progression in NB tumors. These observations suggest that reactivation of the accumulated Noxa in the Doxo-resistant NB cells with p53-independent stress may provide a new therapeutic approach to chemotherapy-resistant NB. Moreover, biochemical analysis of the accumulated Noxa in the mitochondria of resistant cells, for example, the analysis of Noxa-binding Bcl-2-family proteins in mitochondria, may be useful to address the mechanism of the failure of Doxo-induced apoptosis in those cells.

To address the other potential mechanisms of the resistances of DNA-damage-induced reagents in the chosen cell lines, we studied the genomic amplification of *MYCN* (Materials and methods), *caspase-8* and *P-glycoprotein* mRNA expression by semi-quantitative RT–PCR (data not shown). Caspase-8 was expressed in NB-9, NB-69, SK-N-SH and NB-1 cells. However, caspase-8 seems not to have a significant role in the Doxo-induced NB apoptosis, since we could not detect its activation by western blotting (data not shown). P-glycoprotein was clearly expressed in NB-9, NB-69, SK-N-SH and NB-1 cells, but not in SH-SY5Y, NB-1, and IMR32 cells (data not shown), suggesting that p-glycoprotein seems not to relate to the Doxo sensitivity of NB cells. Regarding *MYCN* amplification status, all the three resistant cell lines had *MYCN* amplification and three of four sensitive cell lines had single copy *MYCN*, suggesting that inactivity of p53 in the resistant cell lines may relate to the *MYCN* amplification. Consistent with our observation, Bell *et al.* (2006) reported that *MYCN* amplification correlates with attenuated $p21^{Cip1/Waf1}$ induction in *p53* wild-type NB cells. The analysis of the molecular mechanism between *MYCN* amplification and p53 inactivation in NB cells may be important for NB studies.

Taken together, our findings indicate that the p53 pathway regulates NB cell apoptosis via pro-apoptotic Noxa kinetics and localization in the mitochondria. Further study of Noxa in NB may provide an important approach to develop new therapies for NB and to improve the prognosis of high-risk NB patients.

Materials and methods

Reagents and antibodies

Anti-p53 mouse monoclonal antibody (clone DO-1), anti-Bcl-2 mouse monoclonal antibody (clone C-2), anti-$p21^{Cip1/Waf1}$ mouse monoclonal antibody (clone F-5) and anti-Bad mouse monoclonal antibody (clone C-7) were from Santa Cruz Biotechnology Inc. (Santa Cruz, CA, USA). Anti-cytochrome-*c* mouse monoclonal antibody (clone 7H8.2C12), anti-Bcl-xL mouse monoclonal antibody (clone 2H12), anti-caspase-3 rabbit polyclonal antibody, anti-caspase-7 mouse monoclonal antibody (clone B94-1) and anti-Bid rabbit polyclonal antibody were from BD PharMingen (San Diego, CA, USA). Anti-phospho-p53 rabbit serum (p53ser15p, p53ser20p and p53ser46p) and anti-phospho-p53ser15 mouse monoclonal antibody (clone 16G8) were from Cell Signaling Technology (Beverly, MA, USA). Anti-Bax and Anti-Bak rabbit polyclonal antibodies were from Upstate Biotechnology (Lake Placid, NY, USA). Anti-p53 mouse monoclonal antibody (clone pAb421), anti-p53 sheep polyclonal Antisera (Ab-7) Kit and anti-Noxa mouse monoclonal antibody (clone 114C307, for immunofluorescence analysis) were from Oncogene Research Products (Cambridge, MA, USA). Anti-Noxa rabbit polyclonal antibody (for western blotting) was from Abcam (Cambridge, UK). Anti-Bim rabbit polyclonal antibody was from Millennium Biotechnology (Ramona, CA, USA). Anti-Bok rabbit polyclonal antibody was from ABGENT (San Diego, CA, USA). Anti-caspase-9 mouse monoclonal antibody (clone 5B4) was from MBL (Nagoya, Japan). Anti-lamin monoclonal antibody (clone JOL2) was from Chemicon (Temecula, CA, USA). Anti-β-tubulin mouse monoclonal antibody (clone KMX-1) was from Roche Diagnostics (Manheim, Germany). Anti-trifunctional protein serum was prepared by rabbit immunization and affinity selection with purified trifunctional protein (Kamijo *et al.*, 1993). Anti-HDM2 monoclonal antibody (clone 2A10) was a generous gift from Dr Arnold J Levine, Pediatrics and Biochemistry Cancer Institute of New Jersey. Other biochemical reagents were purchased from Sigma-Aldrich Japan, or Wako (Osaka, Japan).

Cells and cell culture

We collected p53 wild-type NB cell lines to study the role of the p53 pathway in drug resistance mechanism of NB cells. SK-N-SH, NB-9, NB-19 and NB69 were obtained from Riken Cell Bank (Tsukuba, Japan). IMR32 and NB-1 were from Cell Resource Center for Biomedical Research Institute of Development, Aging and Cancer, Tohoku University. The wild-type *p53*-expressing SH-SY5Y line was purchased from ATCC (Manassas, VA, USA). The wild-type p53 status was demonstrated in previous reports (IMR32: Hopkins-Donaldson *et al.*, 2002; SK-N-SH: Wolff *et al.*, 2001) and p53 sequencing, which was performed according to the previous report (Tweddle *et al.*, 2001), confirmed the wild-type p53 status in these cell lines. In terms of the copy number of MYCN by Southern blot analysis, SH-SY5Y, SK-N-SH and NB-69 are single-copy NB cells; NB-9, IMR32, NB-1 and NB-19 cells have 50, >150, >150 and 25 copies, respectively (data not shown). The cells were routinely maintained with DMEM supplemented with 10% fetal bovine serum (FBS) and 1 × penicillin/streptomycin (Invitrogen, Carlsbad, CA, USA).

Tumor samples

Fresh, frozen tumor tissues were sent to the Division of Biochemistry, Chiba Cancer Center Research Institute, from various hospitals in Japan with informed consent from the patients' parents. All samples were obtained by surgery or biopsy and stored at −80°C. More than 70% of tumor cell contents of the samples were confirmed by pathological analysis of the adjacent tissues. Studies were approved by the Institutional Review Board of the Chiba Cancer Center.

Cell proliferation assay

NB cells were seeded in 96-well plates at a density of 10^4 cells/well in a final volume of 100 μl. Twenty-four hours after seeding, the medium was removed and replaced with fresh medium or with medium containing 0.5 μg/ml of Doxo or 20 μM etoposide in a final volume of 100 μl. The culture was maintained in the 5% CO_2 for 24 h and then 10 μl of WST-8 labeling solution (Cell Counting Kit-8, DOJINDO, Kumamoto, Japan) was added, and the cells were returned to the incubator for 4 h. The absorbance of the formazan product formed was

Table 1 Sequence of primers for PCR experiments

Gene	*Forward primer sequence*	*Reverse primer sequence*	*Accession number*
p53	cagccaagtctgtgacttgcacgtac	ctatgtcgaaaagtgtttctgtcatc	NM_000546
$p21^{Cip1/Waf1}$	gacaccactggagggtgact	ggcgtttggagtggtagaaa	L25610
HDM2	tagtagcattatttatagcagcc	agagaagaaatctatgtgaattgag	Z12020
Noxa	agagctggaagtcgagtgt	gcaccttcacattcctctc	D90070
Bax	ttttgcttcagggtttcatc	cagttgaagttgccgtcaga	BC014175
Bak1	gcctttgcagttggactctc	gggttgggagcaagtgtcta	NM_001188
IFN-α1	caatatctacgatggcctcgc	agagatggctggagccttctg	NM_024013
Caspase-8	gggacaggaatggaacacac	gccatagatgatgcccttgt	AF009620
P-glycoprotein	gaatctggaggaagacatgacc	tccaattttgtcaccaattcc	NM_000927
G3PDH	accacagtccatgccatcac	tccaccaccctgttgctgta	NM_002046

detected at 450 nm in a 96-well spectrophotometric plate reader, as per the manufacturer's protocol.

Morphological analysis of apoptosis and analysis of sub-G_0/G_1 fraction

Cells were observed using a phase-contrast microscope to assess apoptotic morphological changes and treated with 4′,6-diamidino-2-phenylindole (DAPI), a DNA-staining dye, to detect the morphological characteristics of apoptotic nuclei, namely, condensation and fragmentation, after fixation with 3.7% (v/v) formaldehyde/1 × phosphate-buffered saline (PBS). Analysis of sub-G_0/G_1 fraction was performed by using the method described in the previous report (Nakazawa *et al*., 2003).

Immunofluorescence

Fixation was performed with 3.7% (v/v) formaldehyde/1 × PBS for 30 min and the permeabilization was done with 0.1% (v/v) TritonX-100/1 × PBS for 5 min at room temperature. Cells were then stained for 1 h with the first antibody followed by a 30-min exposure to an appropriate second antibody conjugated with fluorescent dye (Alexa488 or Alexa594). DNA was visualized with DAPI or propidium iodide. Analysis by confocal laser microscopy was performed with an LSM510 system (Carl Zeiss, Oberkochen, Germany).

Cell fractionation and direct western blotting

For the isolation of the heavy membrane faction (Mito) in Figures 4A and B, 2×10^6 cells were subjected to the fractionation procedure described previously (Nakazawa *et al*., 2003). The resulting supernatant after isolation of Mito was referred to as the cytosol plus light membrane (Cyto) fractions.

For isolation of the nucleus (Nuc) in Figure 2d, 1×10^6 cells were suspended in 0.4 ml of buffer (10 mM HEPES pH 7.9, 10 mM KCl, 1.5 mM $MgCl_2$, 0.5 mM DTT, 0.4 μM PMSF), and incubated on ice for 20 min. After vortexing for 1 min at the maximum setting, cells were centrifuged at 15 000 r.p.m. for 10 s, and then the supernatant was kept as cytosol (Cyto). The pellet was resuspended in 0.1 ml of buffer (20 mM HEPES pH 7.9, 420 mM NaCl, 1.5 mM $MgCl_2$, 0.2 mM EDTA, 25% (v/v) glycerol, 0.5 mM DTT, 0.4 μM PMSF), and incubated on ice for 20 min. Then the cells were centrifuged at 15 000 r.p.m. for 2 min, and then the supernatant was kept as nucleus (Nuc). Direct western blotting was performed according to the previous report (Nakazawa *et al*., 2003).

Preparation of mRNA and analysis of RNA expression

Total RNA was extracted from NB cells using Isogen (Wako, Tokyo, Japan), and cDNA was synthesized from 1 μg of total RNA templates according to the manufacturer's protocol (RiverTra-Ace-α- RT–PCR kit, TOYOBO, Osaka, Japan). PCR amplification of either p53 or Noxa was performed using previously reported primers (for p53: Paull and Whikehart, 2005; for Noxa: Ohtani *et al*., 2004). The other primer sequences are listed in Table 1. RT–PCR products (~0.5 kb) were detected by direct ethidium bromide staining after electrophoretic separation on agarose gels. RT–PCR analysis of G3PDH mRNA expression was performed as a positive control for these experiments according to the manufacturer's protocol (RiverTra-Ace -α- RT–PCR kit). Semi-quantitative RT–PCR analysis of tumor samples was performed according to the previous report (Machida *et al*., 2006). The PCR amplification was performed using the above-mentioned primers for Noxa.

Quantitative real-time PCR analysis

For quantification of Noxa in primary NB samples, cDNA was synthesized with random primers Superscript II reverse transcriptase (GibcoBRL) from 15 μg of primary tumor total RNA. Noxa and GAPDH primers and probes were purchased from Applied Biosystems (Noxa Assay ID: Hs00560402_m1; GAPDH: Pre-Developed TaqMan Assay Reagents Human G3PDH). Quantitative real-time PCR analysis was performed by ABI7700 Prism sequence detector (Applied Biosystems, Foster City, CA, USA), according to the manufacturer's instructions using 1 × TaqMan Universal PCR Master Mix. After denaturing at 95°C for 10 min, PCR amplification was performed by 50 cycles of denaturation at 95°C for 15 s and annealing/extension at 60°C for 1 min. A quantification of *Noxa* mRNA in each sample was performed by comparing with the standard curve, which was generated by reacting the plasmid containing human Noxa (Hijikata *et al*., 1990). Furthermore, G3PDH mRNA quantification was also performed for a standardization of the initial RNA content of each sample.

Small interference RNA transfection

Noxa small interference RNAs were synthesized according to the previous experiments (Noxa siRNA1, Qin *et al*., 2004: 5′-TCAGTCTACTGATTTACTGG-3′; Noxa siRNA2, Lee *et al*., 2005: 5′-AACTTCCGGCAGAAACTTCTG-3′). Control siRNA (Silencer Negative Control #1 siRNA) was purchased from Ambion Inc. (Austin, TX, USA). NB cells were plated at a density of 3×10^5 cells in a 3-cm-diameter dish. Small interference RNA duplexes (10 nM) were transfected with Lipofectamine™ RNAiMAX in Opti-MEM medium according to the manufacturer's protocol. After 24 h, transfected cells were treated with Doxo for another 24 h.

Statistical analysis

The Welch test was used as a statistical method of parametric test to explore possible associations between Noxa expression and other factors, using StatView ver. 4.11 (Abacus Concepts

Inc., Cheltenham, UK). Statistical significance was declared if the *P*-value was <0.05.

Acknowledgements

We are deeply indebted to Professor Kenichi Koike (Department of Pediatrics, Shinshu University School of Medicine) for his excellent advice. We thank Kumiko Sakurai, Yozo Nakazawa, and Jun Miki for their technical assistance, and Daniel Mrozek, Medical English Service Inc, for editorial assistance. This work was supported by grants from the Japanese Ministry of Education, Science, Sports and Culture, Grant-in-Aid for Scientific Research (C) (contract nos: 15591098 and 17591077).

References

Aleyasin H, Cregan SP, Iyirhiaro G, O'Hare MJ, Callaghan SM, Slack RS *et al.* (2004). Nuclear factor-(kappa)B modulates the p53 response in neurons exposed to DNA damage. *J Neurosci* **24**: 2963–2973.

Bell E, Premkumar R, Carr J, Lu X, Lovat PE, Kees UR *et al.* (2006). The role of MYCN in the failure of MYCN amplified neuroblastoma cell lines to G1 arrest after DNA damage. *Cell Cycle* **5**: 2639–2647.

Danial NN, Korsmeyer SJ. (2004). Cell death: critical control points. *Cell* **116**: 205–219.

Green DR. (2000). Apoptotic pathways: paper wraps stone blunts scissors. *Cell* **102**: 1–4.

Hempel G, Flege S, Wurthwein G, Boos J. (2002). Peak plasma concentrations of doxorubicin in children with acute lymphoblastic leukemia or non-Hodgkin lymphoma. *Cancer Chemother Pharmacol* **49**: 133–141.

Hijikata M, Kato N, Sato T, Kagami Y, Shimotohno K. (1990). Molecular cloning and characterization of a cDNA for a novel phorbol-12-myristate-13-acetate-responsive gene that is highly expressed in an adult T-cell leukemia cell line. *J Virol* **64**: 4632–4639.

Hopkins-Donaldson S, Yan P, Bourloud KB, Muhlethaler A, Bodmer JL, Gross N. (2002). Doxorubicin-induced death in neuroblastoma does not involve death receptors in S-type cells and is caspase-independent in N-type cells. *Oncogene* **21**: 6132–6137.

Hudson CD, Morris PJ, Latchman DS, Budhram-Mahadeo VS. (2005). Brn-3a transcription factor blocks p53-mediated activation of proapoptotic target genes Noxa and Bax *in vitro* and *in vivo* to determine cell fate. *J Biol Chem* **280**: 11851–11948.

Isaacs JS, Saito S, Neckers LM. (2001). Requirement for HDM2 activity in the rapid degradation of p53 in neuroblastoma. *J Biol Chem* **276**: 18497–18506.

Kamijo T, Aoyama T, Miyazaki J, Hashimoto T. (1993). Molecular cloning of the cDNAs for the subunits of rat mitochondrial fatty acid beta-oxidation multienzyme complex. Structural and functional relationships to other mitochondrial and peroxisomal beta-oxidation enzymes. *J Biol Chem* **268**: 26452–26460.

Keshelava N, Zuo JJ, Chen P, Waidyaratne SN, Luna MC, Gomer CJ *et al.* (2001). Loss of p53 function confers high-level multidrug resistance in neuroblastoma cell lines. *Cancer Res* **61**: 6185–6193.

Kiryu-Seo S, Hirayama T, Kato R, Kiyama H. (2005). Noxa is a critical mediator of p53-dependent motor neuron death after nerve injury in adult mouse. *J Neurosci* **25**: 1442–1447.

Komarova EA, Chernov MV, Franks R, Wang K, Armin G, Zelnick CR *et al.* (1997). Transgenic mice with p53-responsive lacZ: p53 activity varies dramatically during normal development and determines radiation and drug sensitivity *in vivo*. *EMBO J* **16**: 1391–1400.

Letai A, Bassik MC, Walensky LD, Sorcinelli MD, Weiler S, Korsmeyer SJ. (2002). Distinct BH3 domains either sensitize or activate mitochondrial apoptosis, serving as prototype cancer therapeutics. *Cancer Cell* **2**: 183–192.

Lee SJ, Kim KM, Namkoong S, Kim CK, Kang YC, Lee H *et al.* (2005). Nitric oxide inhibition of homocysteine-induced human endothelial cell apoptosis by down-regulation of p53-dependent Noxa expression through the formation of S-nitrosohomocysteine. *J Biol Chem* **280**: 5781–5788.

Lowe SW, Bodis S, McClatchey A, Remington L, Ruley HE, Fisher DE *et al.* (1994). p53 status and the efficacy of cancer therapy *in vivo*. *Science* **266**: 807–810.

Machida T, Fujita T, Ooo ML, Ohira M, Isogai E, Mihara M *et al.* (2006). Increased expression of proapoptotic BMCC1, a novel gene with the BNIP2 and Cdc42GAP homology (BCH) domain, is associated with favorable prognosis in human neuroblastomas. *Oncogene* **25**: 1931–1942.

Matthay KK, Perez C, Seeger RC, Brodeur GM, Shimada H, Atkinson JB *et al.* (1998). Successful treatment of stage III neuroblastoma based on prospective biologic staging: a Children's Cancer Group study. *J Clin Oncol* **16**: 1256–1264.

Moll UM, LaQuaglia M, Bénard J, Riou G. (1995). Wild-type p53 protein undergoes cytoplasmic sequestration in undifferentiated neuroblastomas but not in differentiated tumors. *Proc Natl Acad Sci USA* **92**: 4407–4411.

Moll UM, Ostermeyer AG, Haladay R, Winkfield B, Frazier M, Zambetti G. (1996). Cytoplasmic sequestration of wild-type p53 protein impairs the G1 checkpoint after DNA damage. *Mol Cell Biol* **16**: 1126–1137.

Nakazawa Y, Kamijo T, Koike K, Noda T. (2003). ARF tumor suppressor induces mitochondria-dependent apoptosis by modulation of mitochondrial Bcl-2 family proteins. *J Biol Chem* **278**: 27888–27895.

Obexer P, Geiger K, Ambros PF, Meister B, Ausserlechner MJ. (2007). FKHRL1-mediated expression of Noxa and Bim induces apoptosis via the mitochondria in neuroblastoma cells. *Cell Death Diff* **14**: 534–547.

Oda E, Ohki R, Murasawa H, Nemoto J, Shibue T, Yamashita T *et al.* (2003). Noxa, a BH3-only member of the Bcl-2 family and candidate mediator of p53-induced apoptosis. *Science* **17**: 1053–1058.

Oda K, Arakawa H, Tanaka T, Matsuda K, Tanikawa C, Mori T *et al.* (2000). p53AIP1, a potential mediator of p53-dependent apoptosis, and its regulation by Ser-46-phosphorylated p53. *Cell* **102**: 849–862.

Ohtani S, Kagawa S, Tango Y, Umeoka T, Tokunaga N, Tsunemitsu Y *et al.* (2004). Quantitative analysis of p53-targeted gene expression and visualization of p53 transcriptional activity following intratumoral administration of adenoviral p53 *in vivo*. *Mol Cancer Ther* **3**: 93–100.

Oren M. (1999). Regulation of the p53 tumor suppressor protein. *J Biol Chem* **274**: 36031–36034.

Paull AC, Whikehart DR. (2005). Regulation of the p53 tumor suppressor protein. *Mol Vis* **11**: 328–334.

Qin JZ, Stennett L, Bacon P, Bodner B, Hendrix MJ, Seftor RE *et al.* (2004). p53-independent NOXA induction overcomes apoptotic resistance of malignant melanomas. *Mol Cancer Ther* **3**: 895–902.

Shen Y, White E. (2001). p53-dependent apoptosis pathways. *Adv Cancer Res* **82**: 55–84.

Shibue T, Takeda K, Oda E, Tanaka H, Murasawa H, Takaoka A *et al.* (2003). Integral role of Noxa in p53-mediated apoptotic response. *Genes Dev* **17**: 2233–2238.

Shieh SY, Ikeda M, Taya Y, Prives C. (1997). DNA damage-induced phosphorylation of p53 alleviates inhibition by MDM2. *Cell* **91**: 325–334.

Tweddle DA, Malcolm AJ, Bown N, Pearson AD, Lunec J. (2001). Evidence for the development of p53 mutations after cytotoxic therapy in a neuroblastoma cell line. *Cancer Res* **61**: 8–13.

Tweddle DA, Pearson AD, Haber M, Norris MD, Xue C, Flemming C *et al.* (2003). The p53 pathway and its inactivation in neuroblastoma. *Cancer Lett* **197**: 93–98.

Wong HK, Fricker M, Wyttenbach A, Villunger A, Michalak EM, Strasser A *et al.* (2005). Mutually exclusive subsets of BH3-only proteins are activated by the p53 and c-Jun N-terminal kinase/c-Jun signaling pathways during cortical neuron apoptosis induced by arsenite. *Mol Cell Biol* **25**: 8732–8747.

Wei MC, Zong WX, Cheng EH, Lindsten T, Panoutsakopoulou V, Ross AJ *et al.* (2001). Proapoptotic BAX and BAK: a requisite gateway to mitochondrial dysfunction and death. *Science* **292**: 727–730.

Wolff A, Technau A, Ihling C, Technau-Ihling K, Erber R, Bosch FX *et al.* (2001). Evidence that wild-type p53 in neuroblastoma cells is in a conformation refractory to integration into the transcriptional complex. *Oncogene* **20**: 1307–1317.

Yakovlev AG, Di Giovanni S, Wang G, Liu W, Stoica B, Faden AI. (2004). BOK and NOXA are essential mediators of p53-dependent apoptosis. *J Biol Chem* **279**: 28367–28374.

Oncogene (2008) 27, 3700–3709

www.nature.com/onc

ORIGINAL ARTICLE

A novel HECT-type E3 ubiquitin protein ligase NEDL1 enhances the p53-mediated apoptotic cell death in its catalytic activity-independent manner

Y Li[1,2,3], T Ozaki[1,3], H Kikuchi[1], H Yamamoto[1], M Ohira[1] and A Nakagawara[1]

[1]*Division of Biochemistry, Chiba Cancer Center Research Institute, Nitona, Chuou-Ku, Chiba, Japan and* [2]*Production Technology Development Center, the Furukawa Electric Co., Ltd., 6 Yawata-Kaigandori, Ichihara, Japan*

NEDL1 (NEDD4-like ubiquitin protein ligase-1) is a newly identified HECT-type E3 ubiquitin protein ligase highly expressed in favorable neuroblastomas as compared with unfavorable ones. In this study, we found that NEDL1 cooperates with p53 to induce apoptosis. During cisplatin (CDDP)-mediated apoptosis in neuroblastoma SH-SY5Y cells, p53 was induced to accumulate in association with an increase in expression levels of NEDL1. Enforced expression of NEDL1 resulted in a decrease in number of G418-resistant colonies in SH-SY5Y and U2OS cells bearing wild-type *p53*, whereas NEDL1 had undetectable effect on *p53*-deficient H1299 and SAOS-2 cells. Similarly, enforced expression of NEDL1 increased number of U2OS cells with sub-G1 DNA content. Co-immunoprecipitation and *in vitro* binding assays revealed that NEDL1 binds to the COOH-terminal region of p53. Luciferase reporter assay showed that NEDL1 has an ability to enhance the transcriptional activity of p53. Small interfering RNA-mediated knockdown of the endogenous NEDL1 conferred the resistance of U2OS cells to adriamycin. It is noteworthy that NEDL1 enhanced pro-apoptotic activity of p53 in its catalytic activity-independent manner. Taken together, our present findings suggest that functional interaction of NEDL1 with p53 might contribute to the induction of apoptosis in cancerous cells bearing wild-type *p53*.

Oncogene (2008) **27**, 3700–3709; doi:10.1038/sj.onc.1211032; published online 28 January 2008

Keywords: apoptosis; cisplatin; DNA damage; HECT-type E3 ubiquitin ligase; NEDL1; p53

Introduction

NEDL1 (NEDD4-like ubiquitin protein ligase-1), which has been identified as a novel gene expressed significantly at high levels in favorable neuroblastomas relative to unfavorable ones, encodes HECT-type E3 ubiquitin ligase and is detected specifically in human neuronal tissues (Miyazaki *et al.*, 2004), suggesting that NEDL1 might be involved in the regulation of the spontaneous regression of favorable neuroblastomas caused by apoptosis and/or neuronal differentiation. According to our previous findings, NEDL1 ubiquitinated mutant forms of SOD1 (superoxide dismutase-1) as well as Dvl-1 (Dishevelled-1), thereby promoting their proteasome-dependent degradation (Miyazaki *et al.*, 2004). SOD1 mutations have been detected in a certain subset of patients with familial amyotrophic lateral sclerosis, which is one of the fatal neurological diseases in human, and mutant SOD1 aggregates to form insoluble macromolecular protein complexes in motor neurons and astrocytes (Cluskey and Ramsden, 2001), suggesting that the accumulation of misfolded proteins generates cellular stresses to induce neuronal cell death. However, the precise molecular mechanisms behind the possible contribution of NEDL1 to apoptosis in motor neurons remain elusive.

As described previously (Gonzalez de Aguilar *et al.*, 2000), pro-apoptotic Bax, which is one of the direct targets of tumor suppressor p53 (Roos and Kaina, 2006), accumulated in central nervous system regions in patients with amyotrophic lateral sclerosis. In support of this notion, p53 was induced in central nervous system regions in patients and also in model mice with amyotrophic lateral sclerosis (Martin, 2000), indicating that p53-mediated pro-apoptotic pathway plays an important role in the regulation of neuronal apoptosis. p53 is a nuclear transcription factor that induces cell cycle arrest and/or apoptosis. Under normal conditions, p53 is kept at extremely low level. The expression of p53 is regulated largely at protein level. For example, E3 ubiquitin ligase MDM2 inhibits transactivation activity of p53 and also promotes its ubiquitination-mediated proteasomal degradation (Vousden and Lu, 2002). In response to genotoxic stresses, p53 is induced to be converted from the latent form to the active one through the post-translational modifications such as phosphorylation and acetylation, and thereby transactivating its direct target genes implicated in cell cycle arrest and/or apoptosis including *p21*^{WAF1}, *MDM2*, *Bax*, *Puma*, *Noxa* and *p53AIP1* (Vousden and Lu, 2002). Accumulating evidence strongly suggests that its transactivation

Correspondence: Dr A Nakagawara, Division of Biochemistry, Chiba Cancer Center Research Institute, 666-2 Nitona, Chuou-Ku, Chiba 260-8717, Japan.
E-mail: akiranak@chiba-cc.jp
[3]These authors contributed equally to this work.
Received 16 May 2007; revised 26 November 2007; accepted 10 December 2007; published online 28 January 2008